Nano-imaging of the beating mouse heart in vivo: Importance of sarcomere dynamics, as opposed to sarcomere length per se, in the regulation of cardiac function

Fuyu Kobirumaki-Shimozawa,[1] Kotaro Oyama,[1,3] Togo Shimozawa,[4] Akari Mizuno,[3] Takashi Ohki,[3] Takako Terui,[2] Susumu Minamisawa,[1] Shin'ichi Ishiwata,[3,5] and Norio Fukuda[1]

[1]Department of Cell Physiology and [2]Department of Anesthesiology, The Jikei University School of Medicine, Minato-ku, Tokyo 105-8461, Japan
[3]Department of Physics and [4]Department of Life Science and Medical Bioscience, School of Advanced Science and Engineering, Waseda University, Shinjuku-ku, Tokyo 169-8555, Japan
[5]Waseda Bioscience Research Institute in Singapore, Waseda University, Helios, Singapore 138667

Sarcomeric contraction in cardiomyocytes serves as the basis for the heart's pump functions in mammals. Although it plays a critical role in the circulatory system, myocardial sarcomere length (SL) change has not been directly measured in vivo under physiological conditions because of technical difficulties. In this study, we developed a high speed (100–frames per second), high resolution (20-nm) imaging system for myocardial sarcomeres in living mice. Using this system, we conducted three-dimensional analysis of sarcomere dynamics in left ventricular myocytes during the cardiac cycle, simultaneously with electrocardiogram and left ventricular pressure measurements. We found that (a) the working range of SL was on the shorter end of the resting distribution, and (b) the left ventricular–developed pressure was positively correlated with the SL change between diastole and systole. The present findings provide the first direct evidence for the tight coupling of sarcomere dynamics and ventricular pump functions in the physiology of the heart.

The Journal of General Physiology

INTRODUCTION

Myocardial sarcomeres undergo repeated cycles of shortening and lengthening in vivo, at a heart rate (HR) dependent on the animal species, and changes in lengths as small as ∼100 nm dramatically change the heart's pump functions (e.g., Allen and Kentish, 1985; Kentish et al., 1986; Kobirumaki-Shimozawa et al., 2014). Therefore, high speed, high resolution imaging of cardiac sarcomeres in vivo is paramount to fully understanding the contributions of sarcomere length (SL) dynamics to cardiac functions under physiological settings.

Recent advances in optical fluorescence technologies have enabled measurements of SL at high spatial and temporal resolution in cardiac cells by using various techniques such as AcGFP expression (i.e., SL nanometry; see Shintani et al., 2014, 2015), quantum dots (Serizawa et al., 2011), and fluorescence staining of the T-tubules (Bub et al., 2010; Botcherby et al., 2013; Ibarra et al., 2013; Inoue et al., 2013). Lee et al. (2012) imaged cardiomyocytes in vivo, as well as coronary arteries, in anesthetized open-chest mice at micron-level resolution, with relatively slow temporal resolution (i.e., one static image obtained during a single cardiac cycle at a fixed Z-direction in the microscope; see also Vinegoni et al., 2015). Recently, Aguirre et al. (2014) captured images of the fluorescence-labeled T-tubules in the mouse heart upon electric stimulation, via two-photon microscopy after reconstruction of the original images (see also Vinegoni et al., 2015). However, large 3-D movements of the heart per se, occurring under physiological settings as compared with skeletal muscle (e.g., Llewellyn et al., 2008, for sarcomere imaging in skeletal muscle in vivo using second harmonic generation), have hindered nano-scale analyses of SL displacement in cardiomyocytes in vivo under physiological settings. In addition, the similarity between the Z-disk spacing (i.e., SL) and T-tubular distance may not be maintained when the heart is at work, especially in a diseased condition (see Guo et al., 2013, and references therein). In the present study, therefore, we developed a high speed, high resolution sarcomere imaging system in the beating mouse heart in vivo and analyzed physiological sarcomere dynamics.

F. Kobirumaki-Shimozawa, K. Oyama, and T. Shimozawa contributed equally to this work.

Correspondence to Fuyu Kobirumaki-Shimozawa: kobirumaki@jikei.ac.jp; or Norio Fukuda: noriof@jikei.ac.jp

Abbreviations used in this paper: ADV, adenovirus; BDM, 2,3-butanedione monoxime; bpm, beats per minute; CaT, Ca^{2+} transient; ECG, electrocardiogram; fps, frames per second; HR, heart rate; LV, left ventricle; LVP, left ventricular pressure; N/A, numerical aperture; SL, sarcomere length.

The Rockefeller University Press $30.00
J. Gen. Physiol. Vol. 147 No. 1 53–62
www.jgp.org/cgi/doi/10.1085/jgp.201511484

MATERIALS AND METHODS

This study was performed in accordance with the Guidelines on Animal Experimentation of The Jikei University School of Medicine. The study protocol was approved by the Animal Care Committee of The Jikei University School of Medicine and the Recombinant Gene Research Safety Committee of The Jikei University School of Medicine.

Adenovirus (ADV) infection in the heart in vivo

3–4-wk-old male BALB/c mice were anesthetized with ∼2% isoflurane (Champion et al., 2003). Next, left thoracotomy was performed by using an electric scalpel (TCU-150; Geiger Medical Technologies) between the third and fourth ribs to visualize the anterior surface of the left ventricle (LV) under ventilation (200 µl at 300 per min). The animal was warmed at ∼38°C (Bio Research Center Co., Ltd.). The ADV solution diluted by PBS (−) (viral titer, 10^{11}–10^{12} particles per ml) was injected into the epicardial surface of the central region of the LV (∼5 µl/mm^2 in ∼10 spots) by using a 1-ml syringe pump (MCIP-BOi; Minato Concept, Inc.) with a 32-gauge needle (Dentronics) under a stereoscopic microscope (SZ61; Olympus) (French et al., 1994; Fromes et al., 1999). One bolus injection of the ADV solution into the epicardial surface of the LV resulted stochastically in the expression of AcGFP in the Z-disks in approximately five cardiomyocytes per injected area. 2 d after chest closure, the mouse was anesthetized again with ∼2% isoflurane and ventilated, and the anterior thoracic wall was removed by cutting the ribs, muscles, and intercostal arteries with the electric scalpel for in vivo cardiac sarcomere imaging. Because AcGFP expression efficacy tends to be higher in relatively young mice (3–4 wk) than in older ones (6–8 wk), we used 3–4-wk-old male BALB/c mice throughout the study.

In vivo sarcomere imaging and hemodynamic recording

The anesthetized open-chest mouse under ventilation was placed on a custom-made microscope stage (250 × 350 mm), and the animal was warmed at 38°C throughout imaging. Electrocardiogram (ECG) lead III was recorded by using an amplifier (JB-611J/MEG-6108/AB-611J; Nihon Kohden) (see Fig. 1, A and B). Likewise, the left ventricular pressure (LVP) was recorded by a catheter (FTH-1211B-0018; Transonic Systems Inc.) inserted from the apex of the heart (Champion et al., 2003). Diastolic LVP was not varied in the present study. A 488-nm laser was used in the confocal unit for the excitation of AcGFP expressed in the Z-disks of cardiomyocytes in the LV of the heart. The ECG and LVP signals and image acquisition timing from the EMCCD camera were simultaneously recorded by LabScribe software (iWorx Systems, Inc.) at 5 kHz. A coverslip (0.04–0.06-mm thick; no. 000; Matsunami Glass Ind., Ltd.) set on a metal ring (diameter, 12 mm) was gently attached at two points (∼2 mm apart) to the LV surface with glue (diameter, ∼2 mm) (see Fig. 1 B). This process was essential to minimize the local myocardial movements (i.e., to maximize the SL analysis resolution) in the targeted imaging region between the glue points. The position of the coverslip was carefully controlled by a custom-made micro-manipulator (Sigma Koki Co.), and then set at the position where the local myocardial movement was suppressed with little or no change in systolic LVP (decrease in systolic LVP of less than ∼5%). The ventilator was turned off during imaging in the experiments shown in Fig. 1 (for ∼10 s); however, it was turned on for the experiments with image sequence reconstruction (see below).

Isolated heart experiment

Experiments were performed as described in our previous study (Inoue et al., 2013). In brief, the heart was isolated from the mouse anesthetized with pentobarbital sodium (100 mg/kg, intraperitoneally), and perfused via the aorta with 5 ml of Ca^{2+}-free HEPES-Tyrode's solution containing 80 mM 2,3-butane-dione monoxime (BDM) at a speed of ∼1 drop/s. Then, the heart was mounted on the custom-made microscope stage, and AcGFP-expressing Z-disks were imaged. In some experiments, CellMask Orange (5 µg/ml in the above solution, 2 ml at a speed of ∼0.5

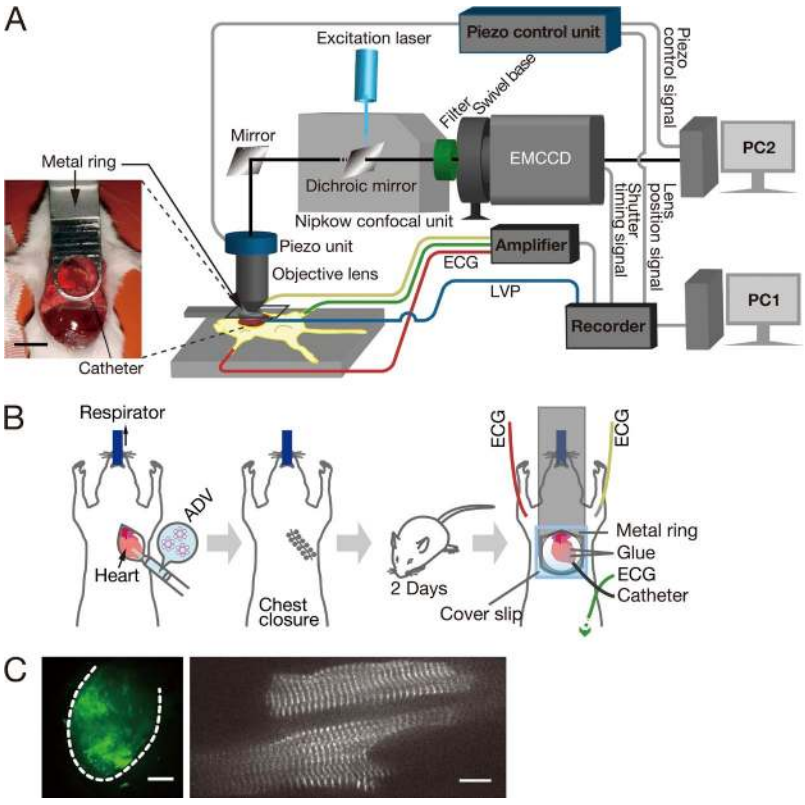

Figure 1. In vivo cardiac sarcomere imaging system. (A) Schematic of the microscopic system. An example of the open-chest mouse is shown on the left (bar, 10 mm). (B) Illustration showing experimental surgery for the expression of α-actinin–AcGFP in the heart in vivo. (C; left) Epi-illumination image of the heart at rest isolated from the mouse with the ADV injection (observed by a 2× lens). Dashed line, outer edge of the heart. Bar, 2 mm. (Right) Confocal image of the myocytes in the isolated perfused heart at rest (observed by a 60× lens). Bar, 10 µm.

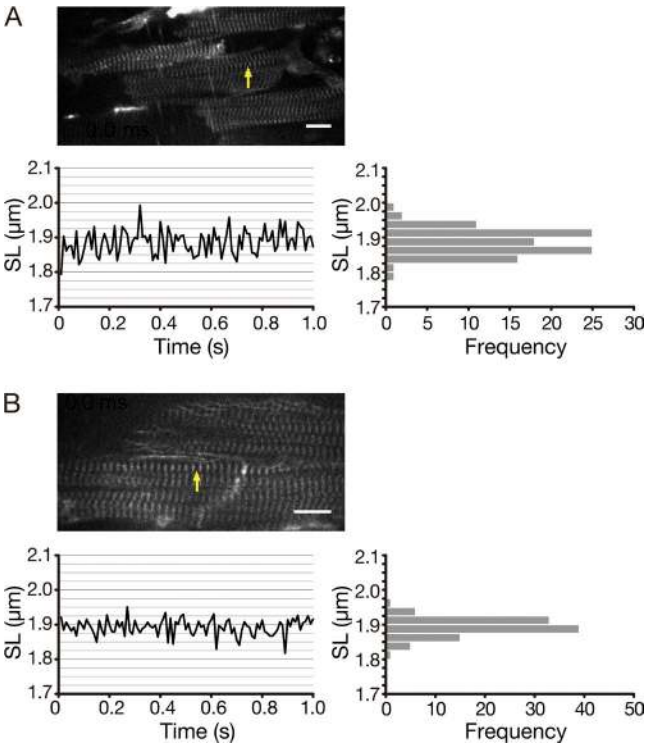

Figure 2. Fluctuation analysis for the length of a single sarcomere in a myocyte in an isolated perfused heart at rest. (A; top) Ventricular myocyte expressed with α-actinin–AcGFP in Z-disks in the isolated heart at rest observed with a 40× lens (N/A, 0.80). (Bottom left) Time course of the change in SL. Imaging performed at 100 fps. (Bottom right) Histogram showing the variance of SL. SD (i.e., an index of single SL displacement resolution; see Serizawa et al., 2011; Shintani et al., 2014, 2015), 40 nm. Yellow arrow, sarcomere used for the SL analysis. (B; top) Ventricular myocyte expressed with α-actinin–AcGFP in Z-disks in the isolated heart at rest observed with a 60× lens (N/A, 1.00). (Bottom left) Time course of the change in SL. Imaging performed at 100 fps. (Bottom right) Histogram showing the variance of SL. SD, 20 nm. In A and B, the hearts were perfused with Ca^{2+}-free HEPES-Tyrode's solution containing 80 mM BDM with little or no LV cavity pressure, hence in diastasis (Inoue et al., 2013). Yellow arrow, sarcomere used for the SL analysis.

drop/s; Life Technologies) was used to stain the T-tubules in ventricular myocytes in the isolated heart. After the treatment with CellMask Orange, the heart was perfused with 5 mL of Ca^{2+}-free HEPES-Tyrode's solution containing 80 mM BDM at a speed of ∼1 drop/s. In this case, the heart was illuminated with a 532-nm laser light (PID-1500; Snake Creek Lasers), and the resultant fluorescence signals (emission filter, BA575IF; Olympus) were detected by the EMCCD camera. A 60× lens (60×W; numerical aperture [N/A] 1.00; LUMPlanFL N; Olympus) was used. Experiments were performed at 25°C.

Reconstruction of image sequences: 3-D scanning microscopy

The objective lens (60×W; N/A 1.00; LUMPlanFL N; Olympus) was moved in the Z-direction by using a piezo-driven nano-positioning device consisting of a piezo flexure objective scanner (P-721 PIFOC; Physik Instrumente GmbH & Co. KG) and a piezo amplifier/servo controller (E-665; Physik Instrumente GmbH & Co. KG) at increments of 1 μm. The EMCCD camera shutter signal was synchronized with ECG, LVP, and the objective lens position (i.e., the Z-direction) by using a four-channel recorder (FA-404; Transonic Scisense Inc., NY). In this experiment, a LVP record was divided into 17 discrete periods (phases), and fluorescence images of a myocyte were obtained in each phase (period, 10.2 ms). The images were then analyzed by a custom-made macro software based on Excel (2010; Microsoft) and ImageJ software, and the best-focused images from phases −8 to 8 were combined to construct an image sequence. SL was measured as stated above by using the multi-peak Gaussian fitting (see Materials and methods in the supplemental text). Because tracking of individual sarcomeres during the course of the cardiac cycle was difficult as a result of a myocyte's XY movements upon heartbeat, the average SL values (17–92 sarcomeres; i.e., 3–11 consecutive sarcomeres in 3–11 different regions within a myocyte) were obtained and used for the analyses.

Statistics

Significant differences were assigned using the paired or unpaired Student's *t* test as appropriate. Data are expressed as mean ± SD unless otherwise noted. Correlation analyses were performed in accordance with the method used in our previous study (Shintani et al., 2014). Statistical significance was assumed to be $P < 0.05$. "NS" indicates $P > 0.05$.

Online supplemental material

Fig. S1 shows our cardiac nano-imaging system. Fig. S2 shows SL changes in the beating heart in vivo in a mouse with high HR. Fig. S3 shows changes in ΔLVP (difference in LVP in diastole and systole) and HR after thoracotomy. Fig. S4 shows sarcomeres in a myocyte in a beating heart in vivo obtained by using image sequence reconstruction. Fig. S5 shows cardiac sarcomere imaging with image sequence reconstruction (as in Fig. S4) in a mouse with high systolic LVP. Video 1 shows a ventricular myocyte in the beating heart in vivo without image sequence reconstruction. Video 2 shows a ventricular myocyte in the beating heart in vivo with image sequence reconstruction. Video 3 shows the myocyte in Video 2 but with no image sequence reconstruction. The online supplemental material is available at http://www.jgp.org/cgi/content/full/jgp.201511484/DC1.

RESULTS

Fig. 1 A illustrates our in vivo cardiac sarcomere imaging system (see also Fig. S1, A and B). Hemodynamic parameters (i.e., ECG and LVP) were simultaneously recorded with real-time sarcomeric motions, and all signals were synchronized by a computer at 5 kHz (PC1 in Fig. 1 A). A 488-nm laser was used for excitation of AcGFP in the beating mouse heart (Fig. 1 A). Fig. 1 B illustrates the preparation of the animal for sarcomere imaging: ADV was injected into the epicardial surface of the LV. 2 d after the viral infection, the mouse was thoracotomized under anesthesia for sarcomere imaging. The ADV injection achieved effective expression of AcGFP in the surface of the LV (see green fluorescence in Fig. 1 C, left), and confocal observation revealed clear banding patterns along the longitudinal axis of the myocytes, indicating that AcGFP expression was localized in sarcomeric Z-disks (Fig. 1 C, right). See the Discussions in the supplemental text.

The AcGFP-expressing myocytes in the isolated perfused heart at rest are shown in Fig. 2. The precision values for the single SL displacement measurement

were 40 and 20 nm with objective lenses of 40× (N/A, 0.80) and 60× (N/A, 1.00), respectively (Fig. 2, A and B). These values were considered to be sufficiently small enough to quantify SL displacement at ∼100-nm levels (see Serizawa et al., 2011; Shintani et al., 2014, 2015).

The experiments based on AcGFP expression using ADV (as well as the fluorescence agent CellMask for staining the T-tubules; see Ibarra et al., 2013; Inoue et al., 2013) in the isolated heart at rest revealed that the resting SL value was 1.97 ± 0.20 µm in the LV (compare Chung and Granzier, 2011) (Fig. 3 A; see Fig. 3, B and C, for the similarity between SL and the T-tubular distance).

We found that sarcomeres regularly repeated shortening and lengthening in synchronization with the movement of the myocyte per se in the beating heart in vivo (Video 1). Fig. 4 A summarizes the typical time-dependent changes in SL in the myocyte during one cardiac cycle. The sarcomeric contraction consisted of shortening followed by relatively slow lengthening, as demonstrated by Iribe et al. (2007) in isolated guinea pig ventricular myocytes in the physiological work-loop style contraction. Multi-peak Gaussian fitting provided the SL values of 2.00 ± 0.11 and 1.72 ± 0.07 µm (n = 5 sarcomeres, as indicated by yellow rectangles in the images in Fig. 4 B, top) in diastole (i) and systole (ii), respectively (hence the shortening ratio, ∼14%). And SL was lengthened to 1.97 ± 0.10 µm in subsequent diastole (iii). Despite the fact that measurements were made in the same myocyte during the cardiac cycle, SL varied by a magnitude of ∼300 nm in both diastolic and systolic phases (see Sarai et al., 2002, for SL variance in isolated rat cardiomyocytes), which is greater than the precision value of 40 nm for SL displacement under the experimental setting (see Fig. 2 A). It should likewise be pointed out that the image was defocused in systole because of the movement of the myocyte along the Z-axis (Fig. 4 B).

Fig. 4 C shows the average values of five consecutive SLs from 29 cardiac cycles obtained from the animal used for Fig. 4 (A and B). Here, we refined the analysis method by developing software based on the two-peak Gaussian fitting, with the aim of quick acquisition of the

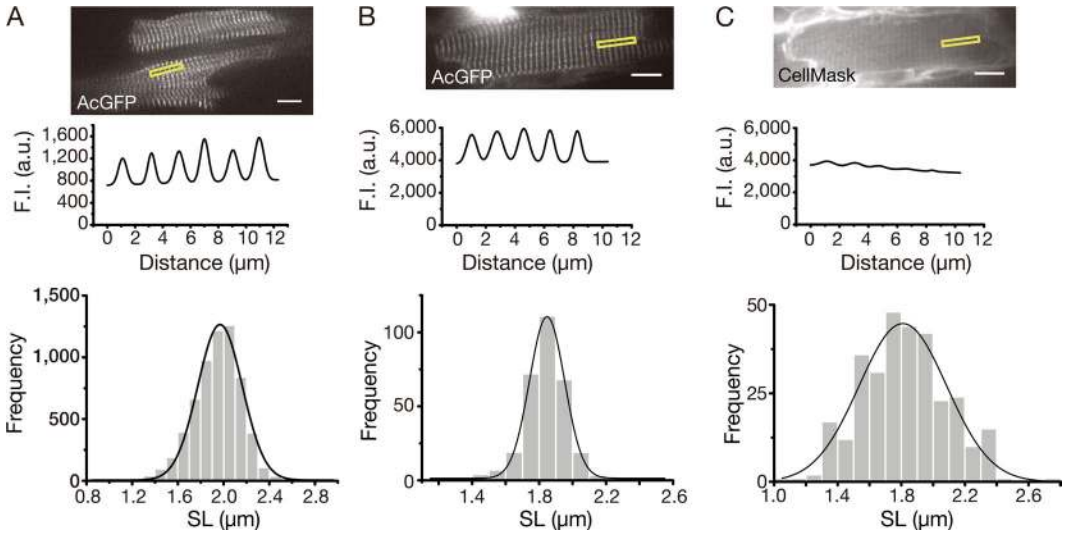

Figure 3. SL variance in myocytes in isolated perfused hearts at rest. (A; top) Typical confocal image of a myocyte expressed with AcGFP in Z-disks via ADV injection. Same as in Fig. 1 C, right. Sarcomeres in the yellow rectangular outline were used for the analysis in the middle trace. Bar, 10 µm. (Middle) Plot profile in the yellow rectangular outline in top. SL, 1.97 ± 0.22 µm. (Bottom) Frequency plot showing SL in myocytes expressed with AcGFP. Data fitted by a single Gaussian function (peak value, 1.97 ± 0.20 µm). Number of sarcomeres analyzed, 6,281 (in 50 myocytes from three hearts). The hearts were perfused with Ca^{2+}-free HEPES-Tyrode's solution containing 80 mM BDM (hence in diastasis; see Inoue et al., 2013), and the myocytes were observed by using appropriate emission filters (see Materials and methods). (B) Striation patterns with AcGFP expression. (Top) Typical confocal image of a myocyte expressed with AcGFP in Z-disks via ADV injection. After isolation, the heart was treated with CellMask according to our previously published procedure (Inoue et al., 2013). Note clear striation patterns along the myocyte (compared with those with CellMask treatment in C). Sarcomeres in the yellow rectangular outline were used for the analysis in the middle trace. Bar, 10 µm. (Middle) Plot profile in the yellow rectangular outline in top. Striation spacing distance (i.e., SL), 1.81 ± 0.05 µm. (Bottom) Frequency plot showing striation spacing distance (i.e., SL) in myocytes expressed with AcGFP. Data fitted by a single Gaussian function (peak value, 1.85 ± 0.10 µm). Number of sarcomeres analyzed, 307 (in seven myocytes from two hearts). (C) Striation patterns with CellMask treatment. (Top) Typical confocal image of a myocyte stained with CellMask at the T-tubules (Inoue et al., 2013). Bar, 10 µm. (Middle) Plot profile in the yellow rectangular outline in top. Striation spacing distance, 1.82 ± 0.13 µm ($P > 0.05$ compared with the data in B, middle). (Bottom) Frequency plot showing the variance of striation spacing distance in myocytes treated with CellMask. Data fitted by a single Gaussian function (peak value, 1.81 ± 0.29 µm). Number of sarcomeres analyzed, 307 (in seven myocytes from two hearts). In both B and C, the hearts were perfused with Ca^{2+}-free HEPES-Tyrode's solution containing 80 mM BDM. And the AcGFP-expressing hearts were treated with CellMask to compare fluorescence intensity between AcGFP and CellMask. The images in B and C were obtained from a different myocyte than that in A.

peak diastolic and systolic SL values (see Materials and methods in the supplemental text for details). As shown in Fig. 4 D, this fitting provided maximal (diastolic) and minimal (systolic) SL values with great ease, from the data of multiple cardiac cycles (i.e., 1.93 and 1.73 µm for maximal and minimal values, respectively, from 29 cardiac cycles in the animal used for Fig. 4 C). Accordingly, experiments using 13 mice demonstrated that the SL values averaged 1.90 ± 0.06 and 1.68 ± 0.06 µm in diastole and systole, respectively (i.e., average shortening ratio, ∼12%) (Fig. 4 E). It can therefore be said that under physiological settings in vivo, the working SL range is within the shorter side of the resting SL distribution (i.e., 1.97 ± 0.20 µm; see Fig. 3 A).

We found a significant positive correlation between SL (ΔSL; difference in SL in diastole and systole) and

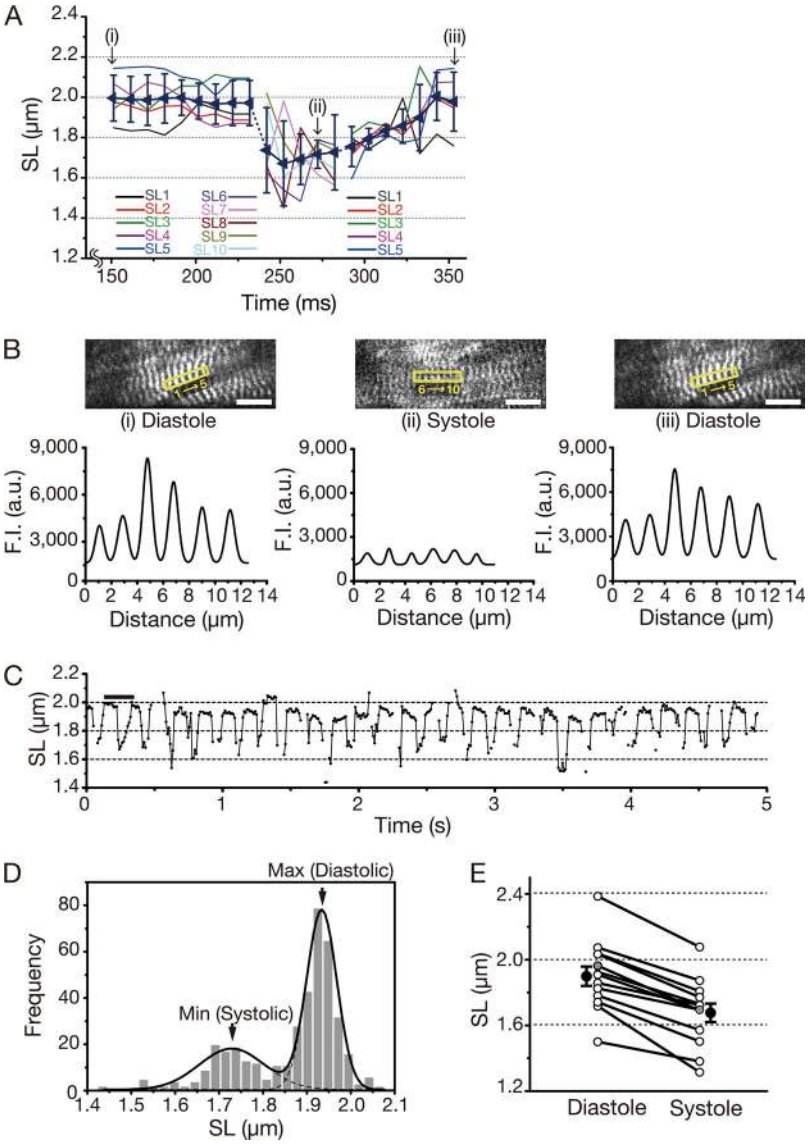

Figure 4. SL changes during the cardiac cycle in vivo. (A) Data showing the time course of changes in SL during the cardiac cycle: i.e., diastole (i), systole (ii), and diastole (iii). Five consecutive sarcomeres in the yellow rectangular outline in the myocyte in B (at [i] 151, [ii] 271, and [iii] 351 ms, as indicated by arrows in the graph) were analyzed. The sarcomeres analyzed in systole differed from those in diastole (hence indicated by different numbers, i.e., 6–10), because of movements of the myocyte associated with heartbeat. Blue triangles indicate average values. Error bars represent mean ± SD (see Materials and methods). Systolic LVP was 49 mmHg, and HR was 251 bpm (both average values from 5 heartbeats before and after the SL data in graph). (B; Top left) Confocal image of the myocyte in diastole (at 151 ms; [i] in A). Sarcomeres numbered from 1 to 5 were analyzed. (Bottom left) Plot profile along the longitudinal axis of the myocyte in top. SL, 2.00 ± 0.11 µm. (Middle top) Confocal image of the myocyte in systole (at 271 ms; [ii] in A). Sarcomeres numbered from 6 to 10 were analyzed. (Middle bottom) Plot profile along the longitudinal axis of the myocyte in top. SL, 1.72 ± 0.07 µm ($P < 0.05$ compared with the value in [i]). (Top right) Confocal image of the myocyte in diastole (at 351 ms; [iii] in A). Sarcomeres numbered from 1 to 5 were analyzed below. Bar, 10 µm. (Bottom right) Plot profile along the longitudinal axis of the myocyte in top. SL, 1.97 ± 0.10 µm ($P < 0.05$ compared with the value in [ii]; $P > 0.05$ compared with the value in [i]). Five consecutive sarcomeres were analyzed in the same myocyte by the multi-peak Gaussian fitting (see Materials and methods in the supplemental text). Length of the myocyte in the image plane, >35 µm throughout the cardiac cycle. Note that the image in the middle (i.e., during systole) was defocused because of movement of the focal point upon cardiac contraction (hence, different numbers were used for sarcomeres). Bar, 10 µm. See Video 1. (C) Typical raw data showing the time course of changes in SL during cardiac cycles. Small black circles indicate the average values of five consecutive sarcomeres at various time points. Data from 29 cardiac cycles obtained from the animal used for A, (B) are shown (bar, data used for the analysis in A; i.e., 151–351 ms). SL values were not analyzed at the time points that the images were out of focus because of movement of the heart (as indicated by the gaps between symbols). (D) Frequency distribution plot for SL (mean of five sarcomeres). The maximal (diastolic) and minimal (systolic) SL values were quantified by fitting the distribution with the combination of two Gaussian functions (see Materials and methods in the supplemental text) (i.e., 1.93 and 1.73 µm for diastolic and systolic SL values, respectively), from 29 cardiac cycles in this animal. Note that the diastolic SL value is slightly different from that obtained in the analysis for B, as a result of fluctuation of diastolic SL (see C). Solid line, combination of two Gaussian functions; dashed line, individual Gaussian functions. (E) Diastolic and systolic SL values obtained by using the two-peak Gaussian fitting in (D) from 13 animals. Average SL values (closed circles) were 1.90 ± 0.06 and 1.68 ± 0.06 µm (mean ± SEM) in diastole and systole, respectively ($P < 0.05$). Thin lines with open circles indicate individual data. Gray symbols indicate the data obtained from the animal in A–D. Error bars represent mean ± SEM.

LVP (ΔLVP; difference in LVP in diastole and systole) within the range of ΔSL from ∼0.1 to ∼0.4 μm (Fig. 5 A), providing direct evidence that changes in SL at ∼100-nm levels significantly affect the heart's pump functions. When ΔLVP was plotted against the percent SL shortening ratio, a significant correlation was likewise observed (Fig. 5 B). However, no correlation was found between diastolic SL or systolic SL and ΔLVP (Fig. 5, C and D), suggesting that ΔSL (or SL shortening ratio) is the most reliable index reflecting myocardial contractility in vivo. HR varied between ∼250 and ∼550 beats per minute (bpm) in the present study; however, no significant correlation was found with ΔLVP (Fig. 5 E).

Fig. S2 shows an α-actinin–AcGFP–expressing myocyte in a mouse showing the highest HR value in Fig. 5 (i.e., 523 bpm). Striations were clearly observed in both systole and diastole, with distinct SL shortening, indicating the capability of our imaging system to derive SL values from mice with various HR values. It is likewise worthwhile noting that our imaging system is potentially applicable to animals with a more rapid HR of 600–700 bpm, because of the imaging rate (i.e., 100 frames per second [fps]) being ∼10 times higher than these values.

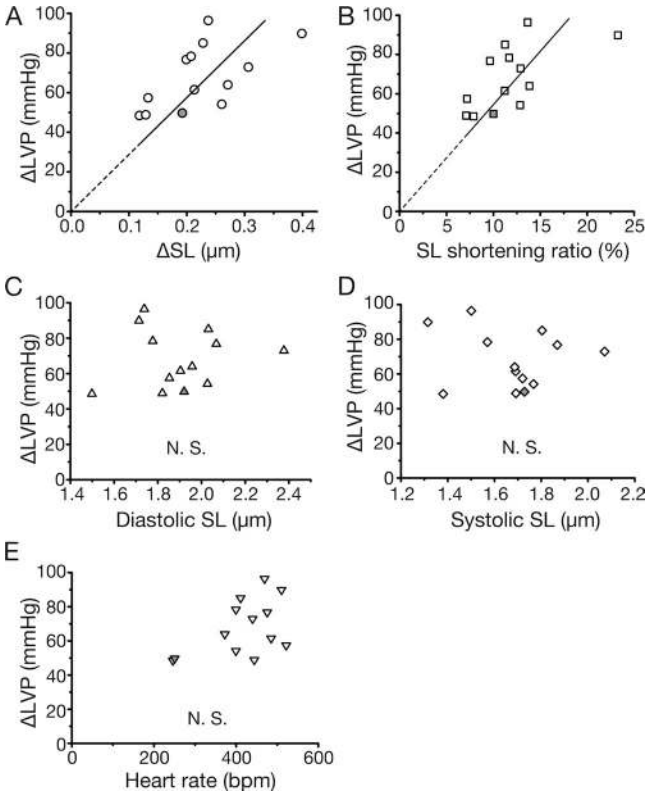

Figure 5. Relationships of ΔLVP versus various parameters. (A) Relationship between ΔSL and ΔLVP from the animals in Fig 4 E. Each plot was obtained from one animal with the average values of ΔSL and ΔLVP (analyzed from 10–30 cardiac cycles). A significant positive correlation ($Y = 287.3X$) was present ($P < 0.05$; $R = 0.60$). (B) SL shortening ratio (%) plotted against ΔLVP. The shortening ratio was obtained by ΔSL (diastolic SL minus systolic SL) divided by diastolic SL. A significant positive correlation ($Y = 5.4X$) was present between parameters ($P < 0.05$; $R = 0.62$). (C) Diastolic SL plotted against ΔLVP. No significant correlation existed between parameters. (D) Systolic SL plotted against ΔLVP. No significant correlation existed between parameters. (E) HR plotted against ΔLVP. No significant correlation existed between parameters. Number of animals, 13. In all panels, gray symbols indicate the data obtained from the animal in Fig. 4, A–D.

In Fig. 4 E, one mouse exhibited extraordinarily short SL values (1.50 and 1.38 μm in diastole and systole, respectively). We conclude that because the mouse was under relatively deep anesthesia with isoflurane, there were exaggerated cardiodepressant effects (see Jensen et al., 1992; Kanaya et al., 1998) after thoracotomy. Indeed, the result of another set of experiments without imaging demonstrated that after thoracotomy, ΔLVP decreased significantly, whereas the HR remained nearly unchanged (Fig. S3).

We then developed a digitally controlled image-reconstruction system. Namely, the position of the objective lens (hence the focal point) was moved downward in the Z-direction at a 1-μm increment by using the piezo actuator (PC2 in Fig. 1 A; see Fig. 6, A and B). After experimentation, the LVP record was divided into 17 phases (i.e., 10.2 ms per phase; indexed from −8 to 8, with the zero point set at its peak); best-focused images were selected at each phase and then combined to obtain an image sequence (Video 2). Video 2 shows clear sarcomeric motions during beating, compared with the original movie obtained in the same animal without image sequence reconstruction (Video 3). As confirmed by the plot profile analysis (Fig. S4, A–D), the images were consistently in focus during the cardiac cycle. Our method likewise revealed that the cardiomyocytes in the epicardial surface of the LV continuously moved in the Z-direction by a magnitude of ∼5 μm during the cardiac cycle (Fig. S4, E and F).

Fig. 6 C summarizes the time course of changes in SL and LVP during the cardiac cycle, obtained by our image-reconstruction system (the myocyte located in the center of the LV). It was found that LVP started to develop (or fall) upon shortening (or lengthening) of SL. The SL shortening ratio was 8% in this mouse, slightly smaller than the average value (i.e., ∼12%) in Fig. 5 B. We consider that the lesser magnitude of the ratio is caused by the relatively low level of systolic LVP in this particular mouse (i.e., ∼40 mmHg in systole; see Fig. 5 with a variance of ΔLVP from ∼40 to ∼100 mmHg). Conversion of the data allowed us to obtain an SL–LVP relationship, clearly showing in vivo that LVP increased (or decreased) upon SL shortening (or lengthening) (Fig. 6 D). As shown in Fig. 6 E, SL was shorter at the peak of systole (phase 0) than in diastole (phase −8), indicating clear contractile motions of sarcomeres during consecutive cardiac cycles within the shorter range

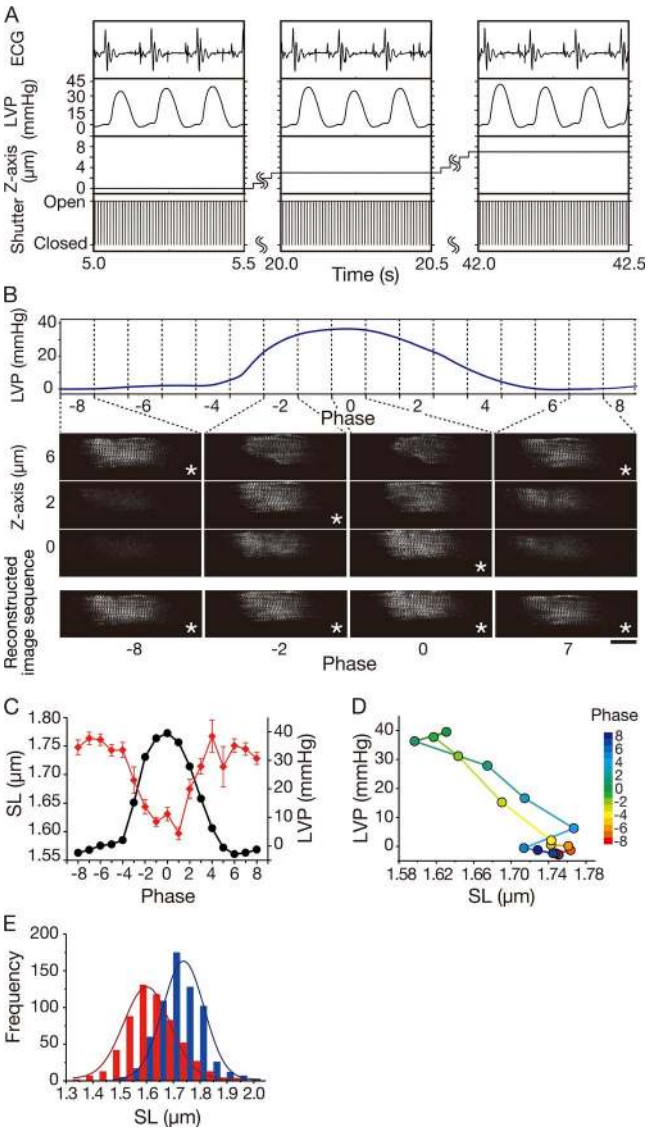

Figure 6. Cardiac sarcomere imaging with image sequence reconstruction. (A) Data showing the method of image sequence reconstruction for in vivo sarcomere imaging. Shown in the following order from top to bottom (analyzed by PC1; see Fig. 1 A): ECG, LVP, objective lens position (along the Z-axis), and EMCCD camera shutter signal (either "open" or "closed" at 100 Hz). Data obtained 5, 20, and 42 s (from left to right) after the onset of recording (0.5 s at each time point). The objective lens position was moved downward by a piezo actuator at a 1-μm increment along the Z-axis; i.e., 0, 3, and 7 μm at 5-, 20-, and 42-s time points, respectively, after the onset of recording (see B for captured static images). HR, ∼400 bpm in this animal throughout the observation. (B; top) Time course of a change in LVP during the cardiac cycle (divided into 17 phases, from −8 to 8, with a period of one phase at 10.2 ms). (Middle) Images of an AcGFP-expressing myocyte in the LV in vivo captured at phases −8, −2, 0, and 7 at 0, 2, and 6 μm in the Z-direction. (Bottom) Best-focused images shown by asterisks in middle. SL was analyzed by using the multiple Gaussian fitting (see Fig. S4, A–D). SL values were 1.75 ± 0.11 (74), 1.64 ± 0.11 (68), 1.63 ± 0.10 (68), and 1.74 ± 0.10 μm (82) at phases −8, −2, 0, and 7, respectively (number of sarcomeres shown in parentheses). Bar, 20 μm. (C) Time-dependent changes in SL (red) and LVP (black) obtained from the analysis in B using the reconstructed image sequence. SL values were averaged at various phases from the reconstructed image sequence. LVP values were averaged at various phases from the data of 546 cardiac cycles (data, mean ± SEM). The values of SD for peak LVP and HR during measurement were less than ∼5 and ∼1%, respectively. (D) Relationship between SL and LVP during the cardiac cycle. Average values of SL and LVP obtained in B were plotted. Colors indicate the phases in the cardiac cycle (as in right). (E) Histograms showing the SL variances at phases −8 (blue) and 0 (red), i.e., in diastole and systole, respectively. The SL values were 1.74 ± 0.08 μm (643 sarcomeres) and 1.60 ± 0.09 μm (583 sarcomeres) at phases −8 and 0, respectively. A similar magnitude of SD was obtained in both phases. Error bars represent mean ± SEM.

of the resting SL distribution (compare Fig. 3 A). Likewise, our 3-D image-reconstruction system could be used to obtain high resolution sarcomere images throughout the cardiac cycle in a mouse with a relatively high systolic LVP (i.e., ∼80 mmHg; see in-focus images in diastole [phase −4] and systole [phase 0] in Fig. S5).

DISCUSSION

In this study, we performed SL nanometry on left ventricular myocytes in living mice, and demonstrated a tight coupling between sarcomere dynamics and ventricular pump functions. Here we discuss the present findings, focusing on the role of sarcomere dynamics in the modulation of ventricular pump functions in vivo.

First, a positive correlation existed between ΔSL (or SL shortening ratio) and ΔLVP (Fig. 5, A and B), but not between diastolic (or systolic) SL and ΔLVP (Fig. 5, C and D). These findings suggest that when data are collected from different individuals, ΔLVP is related to the magnitude of SL change (i.e., ΔSL), at least in the epicardium of the LV, more strongly than to the absolute diastolic SL values in vivo. Consistent with the present findings, a previous study reported no significant correlation between the SL shortening ratio and the absolute resting (=initial [diastolic]) SL in ventricular myocytes isolated from mice (data obtained from 17 mice) (Pohlmann et al., 2007). We consider that these sets of data obtained under different experimental conditions (i.e., in vivo and in myocytes) do not contradict the Frank–Starling law of the heart (see Katz, 2002; Kobirumaki-Shimozawa et al., 2014, and references therein), because the variances in the initial SL and myocardial contractile performance obtained from different individuals are inevitable, and they tend to mask the correlation between the diastolic SL and cardiac contractility.

The positive relationship between ΔSL and ΔLVP may have novel mechanistic implications regarding the relation between the amount of Ca^{2+} released during the Ca^{2+} transient (CaT) and thin filament activation (and the ensuing cross-bridge formation) in myocardium

under auxotonic conditions, as in the beating heart in vivo. It is well established that the activation of thin filaments during the CaT is submaximal, and the occupancy of thin filament sites by myosin molecules never achieves a steady state (e.g., Bers, 2001; Kobirumaki-Shimozawa et al., 2014, and references therein). Therefore, given the brief duration of the CaT (see Tallini et al., 2006, for the CaT in the beating heart), the amount of Ca^{2+} released during the CaT (which is related to the duration of the CaT), rather than the peak value of the CaT, may determine the fraction of the thin filament that switches from the "off" state to the "on" state and thus the kinetics of contraction caused by the activation dependence of the cross-bridge cycling rate (e.g., Kobirumaki-Shimozawa et al., 2014, and references therein). Indeed, it has been reported that the amount of Ca^{2+} released during the CaT affects the on–off equilibrium of the thin filament state and the ensuing cross-bridge cycling rate in myocardium under physiological submaximal activation (e.g., Fitzsimons and Moss, 2007; Moss and Fitzsimons, 2010). Accordingly, it is likely that cross-bridge attachment during the course of the CaT (i.e., sarcomere shortening) can further recruit cross-bridge binding via thin filament cooperative activation, resulting in a positive correlation between ΔSL and cardiac contractility (i.e., ΔLVP; as in Fig. 5 A). We conclude that this cross-bridge–dependent mechanism is relatively stable across species and hence appears in the data from a variety of animals in vivo, because of the constant determinants of myofibrillar contractility across species (e.g., affinity of troponin C for Ca^{2+}, the rate of cross-bridge cycling, and propagation of thin filament cooperative activation via bound cross-bridges). To fully uncover the molecular mechanisms by which the initial SL or the magnitude of SL change (or both) determines cardiac contractility in vivo, it is necessary to simultaneously analyze the ventricular function and Ca^{2+}-dependent sarcomere dynamics in various layers of the heart (i.e., epicardium, midwall, and endocardium) in the same individual mouse at varying levels of ventricular filling by developing high speed, high performance two-photon microscopy. Along this line, it is of importance to investigate in future studies the effects of β-adrenergic stimulation on the relation between ΔSL and ΔLVP (or between diastolic/systolic SL and ΔLVP) in various layers of the ventricle.

The time-dependent changes in SL and LVP, regardless of the level of LVP (Figs. 6 C and S5 A), are qualitatively in good agreement with the findings of previous studies using synchrotron x-ray (Pearson et al., 2004, 2007; Shirai et al., 2013). These researchers applied the x-ray technique to the whole heart by using a high energy source, and developed a new cardiac-imaging technology in that the changes in the intensity ratio (I_{10}/I_{11}; the ratio of thick filament density to thin filament density) in the epicardial surface of the LV were obtained. It was accordingly found that during the cardiac cycle, I_{10}/I_{11} and LVP changed in a reciprocal manner in healthy anesthetized open-chest rats. Moreover, this is reportedly the case for induced pluripotent stem cell–derived cardiomyocytes planted in the epicardial surface of the LV in the anesthetized nude rat (Higuchi et al., 2015). Therefore, the present findings, combined with these lines of previous evidence, support the notion that in the epicardial surface of the central part of the LV wall in rodents, LVP increases (decreases) when sarcomeric contraction commences (terminates) according to the cellular level of the excitation–contraction coupling. The time point for peak SL shortening and that for peak LVP may deviate in other regions, such as in the base or apex, for the ventricle to efficiently eject blood.

Chung and Granzier (2011) reported that passive SL varied in a location-dependent manner in the isolated mouse heart upon barium chloride–induced contraction; SL varied as follows at maximal developed pressure versus no preload (in μm): 2.08 ± 0.01 versus 1.86 ± 0.01, 2.04 ± 0.01 versus 1.80 ± 0.01, and 1.98 ± 0.02 versus 1.73 ± 0.02 in the epicardium, midwall, and endocardium, respectively. We therefore consider that under physiological settings at high heartbeat frequencies in mice in vivo, the working SL range is shifted toward the shorter SL distribution side, presumably as a result of repeated myofibrillar shortening with a short diastolic filling period (thereby causing the difference in the SL measurement in the resting isolated heart and in vivo; compare Figs. 3 A and 4 B). Likewise, because of the nature of the Nipkow confocal scanner, our in vivo cardiac-imaging system enables visualization of the sarcomeric motions in myocytes in the epicardial surface of the ventricle (i.e., restricted to a depth of ∼150 μm because of optical limitations). Therefore, the SL values in myocytes elsewhere (e.g., deeper in the LV wall) may differ from those obtained in the present study in vivo (as reported in Chung and Granzier, 2011).

Because previous studies on cardiac imaging have defined the T-tubular spacing as SL (Bub et al., 2010; Botcherby et al., 2013; Inoue et al., 2013; Aguirre et al., 2014; Vinegoni et al., 2015), we directly compared the Z-disk spacing (i.e., SL) and T-tubular spacing in the present study, and found that SL and the T-tubular spacing showed similar values in the isolated heart at rest (Fig. 3). However, careful consideration must be given, because this similarity may not hold true when the heart is at work. Likewise, the T-tubular geometry relative to the Z-disks may be altered in failing hearts upon structural changes in the T-tubular system (Guo et al., 2013), limiting the application of "T-tubular imaging" in disease models. Moreover, because of the lack of the T-tubular network (Dibb et al., 2013), T-tubular imaging cannot be applied to atrial muscle. Therefore, our real-time nano-imaging of the Z-disks

via expression of α-actinin–AcGFP has a high potential in elucidating the molecular mechanisms of cardiac sarcomere contractility in vivo under various conditions. The image acquisition became difficult in mice with high systolic LVP, primarily because of the movement of the target myocyte along the Z-direction in association with the heartbeat. However, despite that difficulty, the results of mice with low (Fig. 6 C) and high (Fig. S5 A) LVP values suggest that our image-reconstruction system will be useful in the systematic analysis of sarcomere dynamics in mice with various afterload resistance levels, e.g., in disease models.

In conclusion, our cardiac nano-imaging system has yielded direct evidence for the tight coupling between sarcomere dynamics and ventricular contractile function in vivo. The mechanistic implication is that under physiological conditions, the amount of Ca^{2+} released during the CaT is likely to activate thin filaments to a level where myocardial active force is determined by the rate of cross-bridge attachment via continuous thin filament cooperative activation by bound cross-bridges. At relatively high levels of activation, the kinetics of contraction would be expected to be near maximal, as the cross-bridge cycling rate is near maximal (e.g., Moss et al., 2004, and references therein). Thus, in mice, the Frank–Starling mechanism would not be particularly evident, which is the case in the present study. However, it is likely that the Frank–Starling mechanism contributes to a much greater degree in myocardium from larger animals, including humans, as the activation state during a twitch is much less than maximal and thus the cross-bridge cycling rate is lower. Future studies should be designed to systematically and thoroughly investigate the means by which the changes in SL in myocytes in various regions and layers of the myocardium modulate the heart's pump functions in health and disease.

We thank Professor Satoshi Kurihara (The Jikei University School of Medicine) and Professor Hideo Higuchi (The University of Tokyo, Tokyo, Japan) for helpful discussions. We also thank Ms. Naoko Tomizawa (The Jikei University School of Medicine) for technical assistance.

This work was supported in part by Grants-in-Aid for Scientific Research (B) (to N. Fukuda), Challenging Exploratory Research (to N. Fukuda and F. Kobirumaki-Shimozawa), Scientific Research on Innovative Areas (to N. Fukuda), Specially Promoted Research and Scientific Research (S) (to S. Ishiwata), and Research Fellowship for Young Scientists (to K. Oyama) from the Ministry of Education, Culture, Sports, Science and Technology of Japan. This study was also supported in part by Japan Heart Foundation (to F. Kobirumaki-Shimozawa).

The authors declare no competing financial interests.

Author contributions: F. Kobirumaki-Shimozawa, K. Oyama, T. Terui, S. Minamisawa, S. Ishiwata, and N. Fukuda designed the research. F. Kobirumaki-Shimozawa, K. Oyama, and T. Shimozawa developed the microscopic system. T. Shimozawa wrote software. F. Kobirumaki-Shimozawa and T. Ohki designed ADV. F. Kobirumaki-Shimozawa, K. Oyama, and A. Mizuno performed experiments and analyzed the data. F. Kobirumaki-Shimozawa, K. Oyama, T. Shimozawa, and N. Fukuda wrote the manuscript. All authors discussed the results and commented on the manuscript.

Eduardo Rios served as editor.

Submitted: 23 July 2015
Accepted: 16 November 2015

REFERENCES

Aguirre, A.D., C. Vinegoni, M. Sebas, and R. Weissleder. 2014. Intravital imaging of cardiac function at the single-cell level. *Proc. Natl. Acad. Sci. USA.* 111:11257–11262. http://dx.doi.org/10.1073/pnas.1401316111

Allen, D.G., and J.C. Kentish. 1985. The cellular basis of the length-tension relation in cardiac muscle. *J. Mol. Cell. Cardiol.* 17:821–840. http://dx.doi.org/10.1016/S0022-2828(85)80097-3

Bers, D.M. 2001. Excitation–contraction coupling and cardiac contractile force. Kluwer, Dordrecht, Netherlands. 427 pp. http://dx.doi.org/10.1007/978-94-010-0658-3

Botcherby, E.J., A. Corbett, R.A.B. Burton, C.W. Smith, C. Bollensdorff, M.J. Booth, P. Kohl, T. Wilson, and G. Bub. 2013. Fast measurement of sarcomere length and cell orientation in Langendorff-perfused hearts using remote focusing microscopy. *Circ. Res.* 113:863–870. http://dx.doi.org/10.1161/CIRCRESAHA.113.301704

Bub, G., P. Camelliti, C. Bollensdorff, D.J. Stuckey, G. Picton, R.A.B. Burton, K. Clarke, and P. Kohl. 2010. Measurement and analysis of sarcomere length in rat cardiomyocytes in situ and in vitro. *Am. J. Physiol. Heart Circ. Physiol.* 298:H1616–H1625. http://dx.doi.org/10.1152/ajpheart.00481.2009

Champion, H.C., D. Georgakopoulos, S. Haldar, L. Wang, Y. Wang, and D.A. Kass. 2003. Robust adenoviral and adeno-associated viral gene transfer to the in vivo murine heart: Application to study of phospholamban physiology. *Circulation.* 108:2790–2797. http://dx.doi.org/10.1161/01.CIR.0000096487.88897.9B

Chung, C.S., and H.L. Granzier. 2011. Contribution of titin and extracellular matrix to passive pressure and measurement of sarcomere length in the mouse left ventricle. *J. Mol. Cell. Cardiol.* 50:731–739. http://dx.doi.org/10.1016/j.yjmcc.2011.01.005

Dibb, K.M., J.D. Clarke, D.A. Eisner, M.A. Richards, and A.W. Trafford. 2013. A functional role for transverse (t-) tubules in the atria. *J. Mol. Cell. Cardiol.* 58:84–91. http://dx.doi.org/10.1016/j.yjmcc.2012.11.001

Fitzsimons, D.P., and R.L. Moss. 2007. Cooperativity in the regulation of force and the kinetics of force development in heart and skeletal muscles: Cross-bridge activation of force. *Adv. Exp. Med. Biol.* 592:177–189. http://dx.doi.org/10.1007/978-4-431-38453-3_16

French, B.A., W. Mazur, R.S. Geske, and R. Bolli. 1994. Direct in vivo gene transfer into porcine myocardium using replication-deficient adenoviral vectors. *Circulation.* 90:2414–2424. http://dx.doi.org/10.1161/01.CIR.90.5.2414

Fromes, Y., A. Salmon, X. Wang, H. Collin, A. Rouche, A. Hagège, K. Schwartz, and M.Y. Fiszman. 1999. Gene delivery to the myocardium by intrapericardial injection. *Gene Ther.* 6:683–688. http://dx.doi.org/10.1038/sj.gt.3300853

Guo, A., C. Zhang, S. Wei, B. Chen, and L.S. Song. 2013. Emerging mechanisms of T-tubule remodelling in heart failure. *Cardiovasc. Res.* 98:204–215. http://dx.doi.org/10.1093/cvr/cvt020

Higuchi, T., S. Miyagawa, J.T. Pearson, S. Fukushima, A. Saito, H. Tsuchimochi, T. Sonobe, Y. Fujii, N. Yagi, A. Astolfo, et al. 2015. Functional and electrical integration of induced pluripotent stem cell-derived cardiomyocytes in a myocardial infarction rat heart. *Cell Transplant.* In press.

Ibarra, C., J.M. Vicencio, M. Estrada, Y. Lin, P. Rocco, P. Rebellato, J.P. Munoz, J. Garcia-Prieto, A.F.G. Quest, M. Chiong, et al. 2013. Local control of nuclear calcium signaling in cardiac myocytes by perinuclear microdomains of sarcolemmal insulin-like growth factor 1 receptors. *Circ. Res.* 112:236–245. http://dx.doi.org/10.1161/CIRCRESAHA.112.273839

Inoue, T., F. Kobirumaki-Shimozawa, T. Kagemoto, T. Fujii, T. Terui, Y. Kusakari, K. Hongo, S. Morimoto, I. Ohtsuki, K. Hashimoto, and N. Fukuda. 2013. Depressed Frank-Starling mechanism in the left ventricular muscle of the knock-in mouse model of dilated cardiomyopathy with troponin T deletion mutation ΔK210. *J. Mol. Cell. Cardiol.* 63:69–78. http://dx.doi.org/10.1016/j.yjmcc.2013.07.001

Iribe, G., M. Helmes, and P. Kohl. 2007. Force-length relations in isolated intact cardiomyocytes subjected to dynamic changes in mechanical load. *Am. J. Physiol. Heart Circ. Physiol.* 292:H1487–H1497. http://dx.doi.org/10.1152/ajpheart.00909.2006

Jensen, N.F., M.M. Todd, D.J. Kramer, P.A. Leonard, and D.S. Warner. 1992. A comparison of the vasodilating effects of halothane and isoflurane on the isolated rabbit basilar artery with and without intact endothelium. *Anesthesiology.* 76:624–634. http://dx.doi.org/10.1097/00000542-199204000-00021

Kanaya, N., S. Kawana, H. Tsuchida, A. Miyamoto, H. Ohshika, and A. Namiki. 1998. Comparative myocardial depression of sevoflurane, isoflurane, and halothane in cultured neonatal rat ventricular myocytes. *Anesth. Analg.* 87:1041–1047.

Katz, A.M. 2002. Ernest Henry Starling, his predecessors, and the "Law of the Heart". *Circulation.* 106:2986–2992. http://dx.doi.org/10.1161/01.CIR.0000040594.96123.55

Kentish, J.C., H.E. ter Keurs, L. Ricciardi, J.J. Bucx, and M.I. Noble. 1986. Comparison between the sarcomere length-force relations of intact and skinned trabeculae from rat right ventricle. Influence of calcium concentrations on these relations. *Circ. Res.* 58:755–768. http://dx.doi.org/10.1161/01.RES.58.6.755

Kobirumaki-Shimozawa, F., T. Inoue, S.A. Shintani, K. Oyama, T. Terui, S. Minamisawa, S. Ishiwata, and N. Fukuda. 2014. Cardiac thin filament regulation and the Frank-Starling mechanism. *J. Physiol. Sci.* 64:221–232. http://dx.doi.org/10.1007/s12576-014-0314-y

Lee, S., C. Vinegoni, P.F. Feruglio, L. Fexon, R. Gorbatov, M. Pivoravov, A. Sbarbati, M. Nahrendorf, and R. Weissleder. 2012. Real-time in vivo imaging of the beating mouse heart at microscopic resolution. *Nat. Commun.* 3:1054. http://dx.doi.org/10.1038/ncomms2060

Llewellyn, M.E., R.P.J. Barretto, S.L. Delp, and M.J. Schnitzer. 2008. Minimally invasive high-speed imaging of sarcomere contractile dynamics in mice and humans. *Nature.* 454:784–788. http://dx.doi.org/10.1038/nature07104

Moss, R.L., and D.P. Fitzsimons. 2010. Perspectives on: SGP Symposium on Muscle in Health and Disease: Regulation of contraction in mammalian striated muscles—the plot *thick*-ens. *J. Gen. Physiol.* 136:21–27. http://dx.doi.org/10.1085/jgp.201010471

Moss, R.L., M. Razumova, and D.P. Fitzsimons. 2004. Myosin crossbridge activation of cardiac thin filaments: Implications for myocardial function in health and disease. *Circ. Res.* 94:1290–1300. http://dx.doi.org/10.1161/01.RES.0000127125.61647.4F

Pearson, J.T., M. Shirai, H. Ito, N. Tokunaga, H. Tsuchimochi, N. Nishiura, D.O. Schwenke, H. Ishibashi-Ueda, R. Akiyama, H. Mori, et al. 2004. In situ measurements of crossbridge dynamics and lattice spacing in rat hearts by x-ray diffraction: Sensitivity to regional ischemia. *Circulation.* 109:2976–2979. http://dx.doi.org/10.1161/01.CIR.0000133322.19340.EF

Pearson, J.T., M. Shirai, H. Tsuchimochi, D.O. Schwenke, T. Ishida, K. Kangawa, H. Suga, and N. Yagi. 2007. Effects of sustained length-dependent activation on in situ cross-bridge dynamics in rat hearts. *Biophys. J.* 93:4319–4329. http://dx.doi.org/10.1529/biophysj.107.111740

Pohlmann, L., I. Kröger, N. Vignier, S. Schlossarek, E. Krämer, C. Coirault, K.R. Sultan, A. El-Armouche, S. Winegrad, T. Eschenhagen, and L. Carrier. 2007. Cardiac myosin-binding protein C is required for complete relaxation in intact myocytes. *Circ. Res.* 101:928–938. http://dx.doi.org/10.1161/CIRCRESAHA.107.158774

Sarai, N., Y. Kihara, T. Izumi, T. Mitsuiye, S. Matsuoka, and A. Noma. 2002. Nonuniformity of sarcomere shortenings in the isolated rat ventricular myocyte. *Jpn. J. Physiol.* 52:371–381. http://dx.doi.org/10.2170/jjphysiol.52.371

Serizawa, T., T. Terui, T. Kagemoto, A. Mizuno, T. Shimozawa, F. Kobirumaki, S. Ishiwata, S. Kurihara, and N. Fukuda. 2011. Real-time measurement of the length of a single sarcomere in rat ventricular myocytes: a novel analysis with quantum dots. *Am. J. Physiol. Cell Physiol.* 301:C1116–C1127. http://dx.doi.org/10.1152/ajpcell.00161.2011

Shintani, S.A., K. Oyama, F. Kobirumaki-Shimozawa, T. Ohki, S. Ishiwata, and N. Fukuda. 2014. Sarcomere length nanometry in rat neonatal cardiomyocytes expressed with α-actinin–AcGFP in Z discs. *J. Gen. Physiol.* 143:513–524. http://dx.doi.org/10.1085/jgp.201311118

Shintani, S.A., K. Oyama, N. Fukuda, and S. Ishiwata. 2015. High-frequency sarcomeric auto-oscillations induced by heating in living neonatal cardiomyocytes of the rat. *Biochem. Biophys. Res. Commun.* 457:165–170. http://dx.doi.org/10.1016/j.bbrc.2014.12.077

Shirai, M., D.O. Schwenke, H. Tsuchimochi, K. Umetani, N. Yagi, and J.T. Pearson. 2013. Synchrotron radiation imaging for advancing our understanding of cardiovascular function. *Circ. Res.* 112:209–221. http://dx.doi.org/10.1161/CIRCRESAHA.111.300096

Tallini, Y.N., M. Ohkura, B.R. Choi, G. Ji, K. Imoto, R. Doran, J. Lee, P. Plan, J. Wilson, H.B. Xin, et al. 2006. Imaging cellular signals in the heart in vivo: Cardiac expression of the high-signal Ca^{2+} indicator GCaMP2. *Proc. Natl. Acad. Sci. USA.* 103:4753–4758. http://dx.doi.org/10.1073/pnas.0509378103

Vinegoni, C., S. Lee, A.D. Aguirre, and R. Weissleder. 2015. New techniques for motion-artifact-free in vivo cardiac microscopy. *Front. Physiol.* 6:147. http://dx.doi.org/10.3389/fphys.2015.00147